Evolutionary optimization of a Fractional Slot Interior Permanent Magnet motor for a small electric bus

Minos E. Beniakar[a], Athanasios G. Sarigiannidis[b], Panagiotis E. Kakosimos[c] and Antonios G. Kladas[d]

National Technical University of Athens, Faculty of Electrical and Computer Engineering, Laboratory of Electrical Machines and Power Electronics, Zografou, Athens

[a]beniakar@central.ntua.gr, [b]thsarig@central.ntua.gr, [c]panoskak@central.ntua.gr, [d]kladasel@central.ntua.gr

Keywords: Design optimization, differential evolution, finite element method, interior permanent magnet motors, fractional slot concentrated winding, electric vehicles.

Abstract. Fractional Slot Concentrated Winding (FSCW) Interior Permanent Magnet (IPM) motors constitute a favorable choice for electric vehicle applications due to their inherent advantages of high efficiency and performance, field weakening capability and permanent magnet effective shielding from eddy currents. In this paper, an IPM motor with buried sinusoidal magnets for a small electric bus is optimized in terms of both efficiency and performance. The overall magnet volume and the corresponding iron bridge width are maintained within specified borders, thus enabling adequate field weakening and permanent magnet shielding margins. In the optimization process a single-objective Differential Evolution (DE) algorithm is utilized, showing great convergence characteristics.

Introduction

Overall optimization of variable speed traction motors requires a multi-objective analysis in order to account for both performance and efficiency, due to the conflicting nature of the respective criteria. In addition, variable speed traction systems require constant adaptation of torque and speed and thus it is desirable to reduce motor size and weight. Another important issue is the ability of traction motors to demonstrate significant Torque over-Boost and Field Weakening capabilities [1]. This paper introduces a particular single-objective, population-based DE optimization methodology [2,5], facilitating the comparative approach on the rotor geometry optimization of an IPM motor involving FSCW configuration [3]. Design constraints regarding the overall permanent magnet volume and the corresponding iron bridges used to bury the magnets are introduced in order to account for overall weight as well as field weakening and shielding capabilities.

The final optimized motor will be integrated in a commercial diesel mini bus, which will be fully electrified. The respective mini bus model is illustrated in Fig. 1(a). The area where the IPM will be mounted, replacing the diesel engine, is shown in picture 1(b).

(a) (b)

Fig. 1 Application details. (a) Commercial mini bus to be electrified. (b) Mounting area of the IPM.

The necessity for increased torque capability becomes evident, when the vehicle's weight and mass are considered. For the analysis undertaken, the overall magnet volume and the corresponding iron bridge width are maintained within specified borders. This practice renders the control over the overall magnet cost feasible and provides a safety margin regarding the rotor mechanical robustness, as the iron bridges constitute a sensitive part, in terms of manufacturing complexity and reliability. The outer stator radius was maintained less than 30 cm in order to fit in the available mounting area and the inner rotor (shaft) radius was slightly enhanced to further increase the system's mechanical robustness.

Basic Dimensioning

In a first step, an estimation of the motor structure is achieved by considering classical machine design analytical techniques. Such analytical approaches deliver a sub-optimum set of design variables adequately close to the region of the global optimum. The initial design is focused on the satisfaction of the fundamental spatial limitations and operational specifications. The latter are tabulated in Table 1.

Table 1. Basic specifications and dimensions of the IPM

Specification	Nominal load	Overload
Electromagnetic torque (Nm)	>125	>250
Speed (RPM)	4000	8000
Nominal output power (kW)	100	
Nominal phase voltage Amplitude (V)	<150	
Efficiency (%)	>90	
Outer stator radius (mm)	<300	
Motor active length (mm)	<200	

Several important determinants were considered during the preliminary design, and are shown in Fig. 2. The vehicle weight and the wheel radius directly affect the motor specifications regarding speed and torque capability. The vehicle dynamics were utilized to initially determine the nominal values of torque for different operating conditions. The utilized Permanent Magnet (PM) material's properties and its operational characteristics were also taken into account. The PMs constitute the field excitation system and the fact that they are buried in the rotor body incurs a significant field weakening. The most crucial dimensions to be determined are the motor active length L and the air-gap diameter D that constitute the two basic dimensioning variables. Their values were calculated using the basic electrical power capacity formula, which is given by (1).

$$S = 1.11 \cdot k_W \cdot \pi^2 \cdot \overline{B} \cdot ac \cdot D^2 \cdot L \cdot n \tag{1}$$

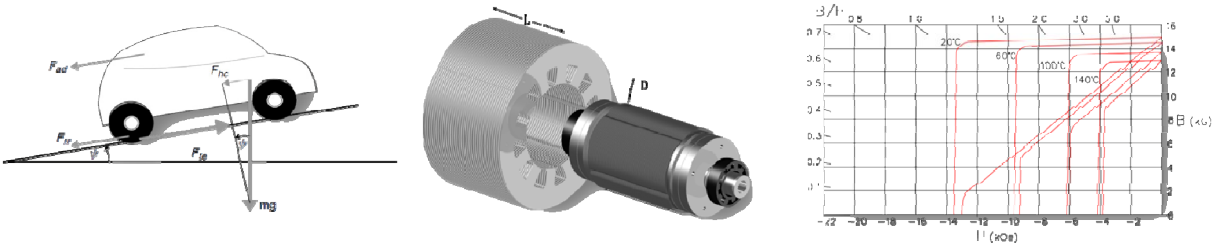

(a) (b) (c)

Fig. 2 Basic considerations regarding the preliminary motor design. (a) Electric vehicle dynamics. (b) Active length- air-gap diameter relationship and (c) Magnetic material properties

The number of poles was dictated by the need for a high speed range operation and the need for relatively low supply frequency in order to minimize iron losses, considering also the higher harmonics in supply voltage and current due to the inverter operation. Generally, in electric vehicle

application a small pole number is employed, most commonly leading to 4 or 8 pole motors [1]. In this specific application a 4-pole rotor was chosen. The number of stator slots was determined analytically, in order to enable optimal electromagnetic coupling of the stator and 4-pole rotor MMF vectors (maximum mean torque). Another consideration was the maximization of the slot fill factor and the minimization of the manufacturing complexity. For this reason the number of stator slots was set equal to 6. The resultant 4/6 FSCW machine offers additional benefits regarding the winding factor and the electromagnetic torque capability.

Optimization Procedure

DE is a population-based optimizer that attacks the starting point problem by sampling the objective function at multiple, randomly chosen initial points. On a first stage, DE perturbs existing vectors with the scaled difference of two randomly selected population vectors to generate new points (mutation). Then, in order to produce the trial vector DE adds the scaled, random vector difference to a third randomly selected population vector (recombination). On a final stage, the trial vector competes against the population vector of the same index (selection). Once the last trial vector has been tested, the survivors of the pair wise competitions become parents for the next generation in the evolutionary cycle. The mutation factor was set equal to F=0.85 and the crossover probability was set equal to FCR=0.8. Forced mutation was used for at least one design variable of every trial vector in order to avoid vector duplication.

The proposed optimization methodology implements a single objective function Differential Evolution optimization routine. The objective function is the weighted sum of different objective functions regarding performance, efficiency and motor clean interface, thus indirectly accounts for multiple objectives [4]. The latter feeds an automated IPM motor design script, generating a 2D Finite Element (FE) model corresponding to each optimization run, thus allowing for precise computation of the objective function values [5]. The flowchart of the DE algorithm is shown in Fig. 3. The block diagram of the overall procedure is illustrated in Fig. 4.

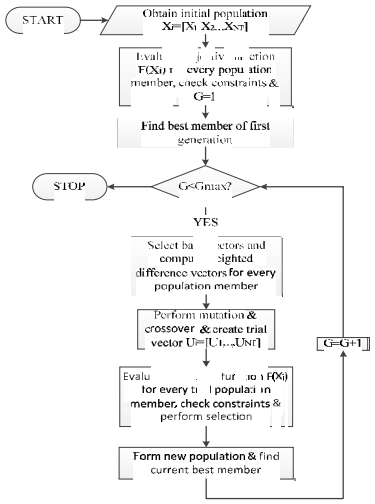

Fig. 3 Flowchart of the proposed optimization algorithm.

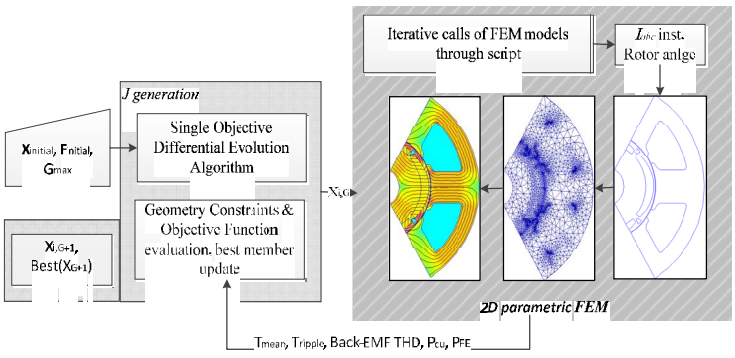

Fig. 4 Optimization procedure block diagram.

The selected design variable vector is given by (1):

$$X_G = \left[k_{\theta\_mag} \quad k_{mag\_\sin} \quad w_{iron\_mag} \right] \tag{1}$$

The ratio of the permanent magnet pitch width to the pole pitch angle k_{θ_mag}, the ratio of the height of the sinusoidal part of the magnet to the height of the radial part of the magnet k_{mag_sin} and

the width of the iron bridge between the magnets and the air-gap w_{iron_mag} have been selected as the three optimization variables, since they play a key-role in terms of both performance and efficiency.

The objective function is given by (2):

$$F = w_1 \cdot \frac{T_{mean,0}}{T_{mean}} + w_2 \cdot \frac{T_{ripple}}{T_{ripple,0}} + w_3 \cdot \frac{THD_{EMF}}{THD_{EMF,0}} + w_4 \cdot \frac{\left(P_{Cu} + P_{Iron}\right)}{\left(P_{Cu} + P_{Iron}\right)_0} \quad (2)$$

It corresponds to maximization of torque capability, minimization of total iron and copper losses and minimization of back-EMF harmonic content and torque ripple, respectively. The index *0* refers to the electromagnetic characteristics of the initial design that occurred from the preliminary analysis.

The flowchart of the general subroutine of the constraints and objective functions handling for the implemented DE algorithm is shown in Fig. 5. The constraints handling strategy is the "death penalty". For every trial vector generated in each generation, constraint functions are evaluated and the potential population member is immediately rejected if at least a single constraint is violated. If none constraint is violated, the objective function for the vector is evaluated and selection is performed. The optimization constraints mostly concerned the preservation of the RMS value of the motor's back-EMF fundamental component below a specific value, dictated by the inverter specifications and the available dc bus. The importance of the consideration of the overall system, including the batteries, in the motor design process is evident. In addition, a minimum of torque capability was considered as a constraint, to preserve solutions enabling increased performance characteristics.

Figure 6 illustrates the evolution of the distribution of the population members in the 3D design variable space for different iteration numbers through the optimization procedure and points out the eventual convergence to a global optimum. The respective projections on the 2D space surfaces are also depicted.

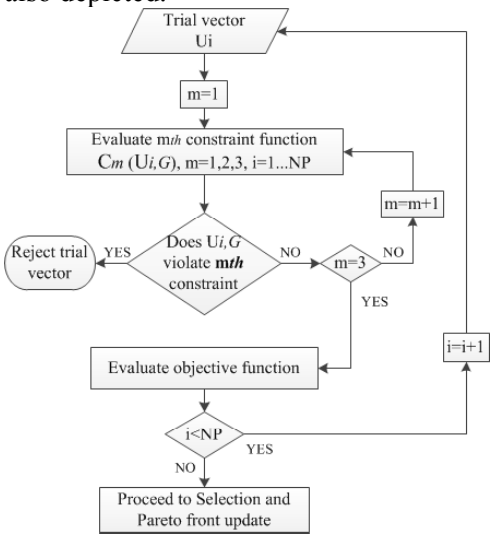

Fig. 5. Flowchart of the constraint and objective function handling procedure

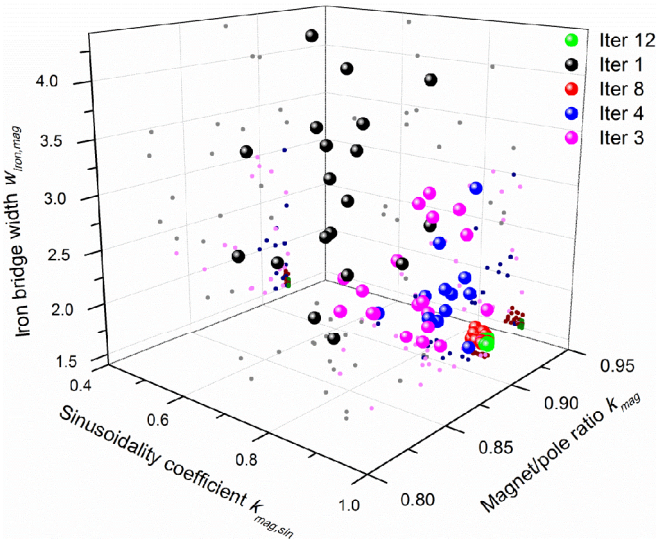

Fig. 6. Evolution of the distribution of the population members in the 3D design variable space

Simulation Results

The variation of the electromagnetic torque and torque ripple and of the fundamental component of the back-EMF respectively, for different values of the design parameters are shown in Fig. 7.

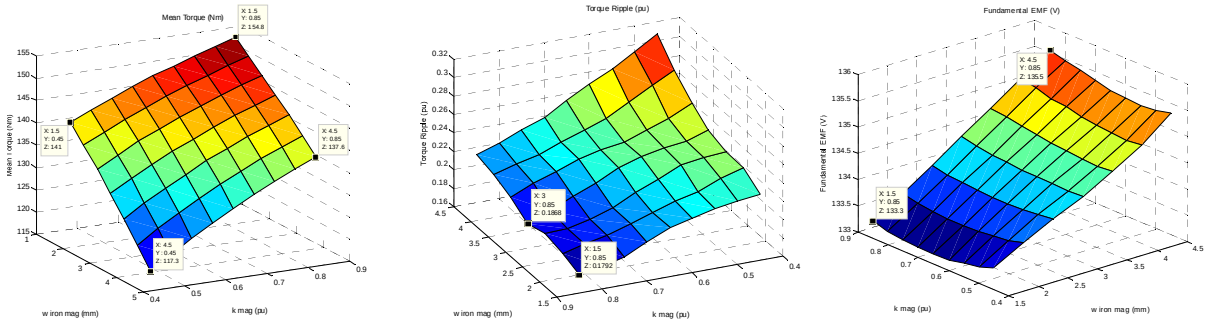

(a) (b) (c)

Fig. 7. Results of the optimization routine. (a) Mean torque – Performance map. (b) Torque ripple map. (c) Back-Emf map

Figure 8 shows the basic operational characteristics of the optimized final motor geometry, under nominal operation. The optimized motor exhibits a very high torque capability and very clean interface regarding the quality of the induced EMF waveform.

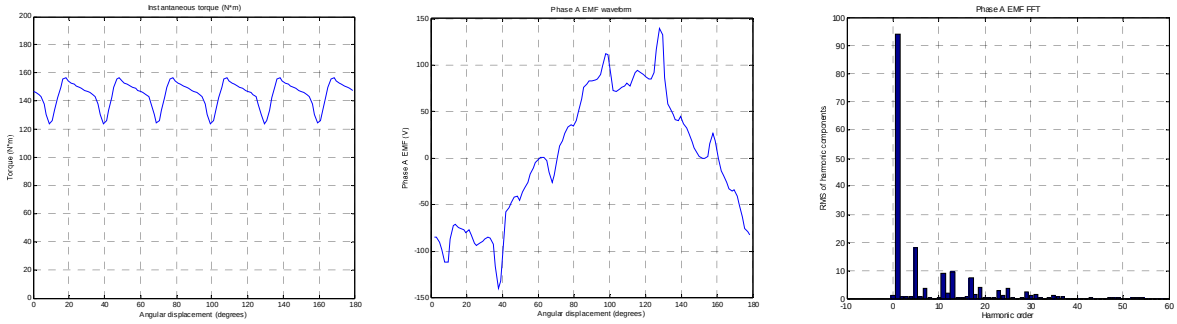

(a) (b) (c)

Fig. 8. Optimized motor characteristics. (a) Electromagnetic torque waveform. (b) Back-EMF waveform. (c) Back-EMF Fourier analysis.

The magnetic field distribution for the final geometry during torque boost and field weakening operation for two different operating conditions, i.e. nominal load and overload is illustrated in Fig. 9 and Fig. 10, respectively.

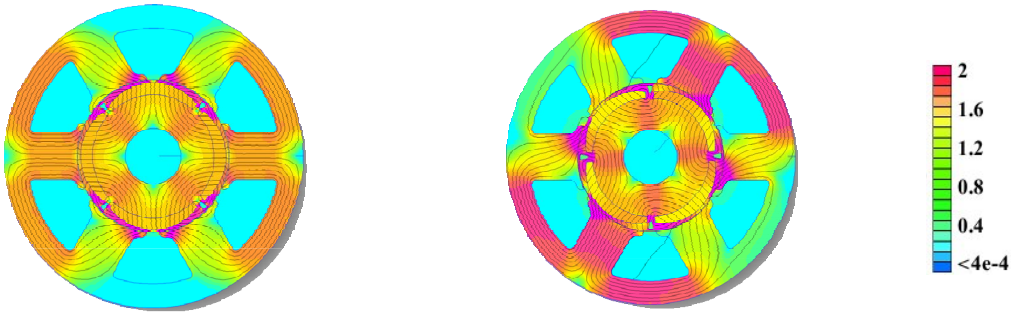

(a) (b)

Fig. 9. Magnetic field distribution for the final geometry during torque boost operation for (a) nominal load. (b) overload.

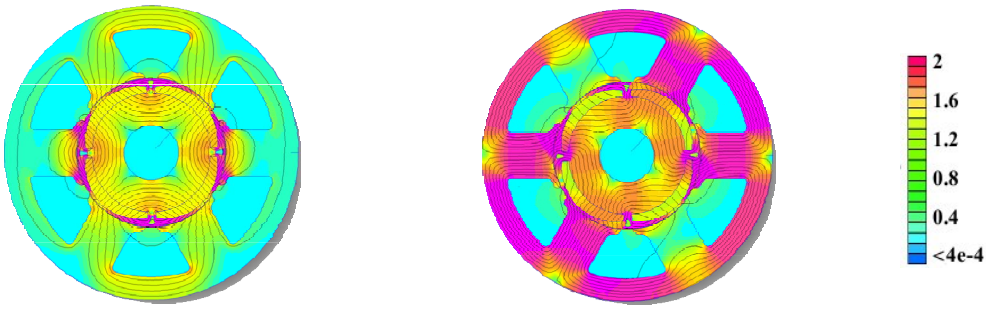

(a) (b)

Fig. 10. Magnetic field distribution for the final geometry during field weakening operation for (a) nominal load. (b) overload.

The final optimized geometry exhibits a torque capability of 144 Nm during nominal load operation and 264 Nm during overload. Its nominal efficiency was estimated, neglecting mechanical losses, over 92%. The induced back-EMF waveforms for both operations present low spatial harmonic content and the RMS values for the fundamental component are 94 V and 102 V respectively.

Conclusions

An efficient DE optimization methodology enabling a comparative approach on the optimization of a FSCW ISM motor for variable speed traction applications has been introduced. Overall motor weight reduction and permanent magnet shielding have been considered, as well as its suitability for different operating conditions. The resulting motor geometry achieves suitable performance-efficiency characteristics.

Acknowledgements

This research has been co-financed by the European Union (European Social Fund - ESF) and Greek national funds under the General Secretariat for Research and Technology of Greece Program: 09ΣΥΝ-51-988 - "Development of electric bus prototype".

References

[1] K. I. Laskaris and A. G. Kladas, "*Optimal Power Utilization by adjusting Torque Boost and Field Weakening Operation in Permanent Magnet Traction Motors*", *IEEE Trans. Energy Convers.*, vol. 27, no. 3, pp. 615-623, Sept. 2012.

[2] M.E. Beniakar, A.G. Sarigiannidis, P.E. Kakosimos and A.G. Kladas, "Multi-objective Evolutionary Optimization of a Surface Mounted PM Actuator with Fractional Slot Winding for Aerospace Applications," *IEEE Trans. Magn., in Press*, DOI 10.1109/TMAG.2013.2285497.

[3] A. Refaie, "*Fractional-Slot Concentrated-Windings Synchronous Permanent Magnet Machines: Opportunities and Challenges*", *IEEE Trans. Ind. Electron.*, Vol. 57, no. 1, pp. 107-121, Jan. 2010.

[4] K. Kim, S. Lim, and D. Koo, "*The shape design of permanent magnet for permanent magnet synchronous motor considering partial demagnetization*", *IEEE Trans. Magn.*, vol. 42, no. 10, pp. 3485–3487, Oct. 2006.

[5] Evangelos M. Tsampouris, Minos E. Beniakar, and Antonios G. Kladas, "*Geometry Optimization of PMSMs Comparing Full and Fractional Pitch Winding Configurations for Aerospace Actuation Applications,*" *IEEE Trans. Magn.,* vol. 48, no. 2, pp. 943-946, February 2012.